# Auto-digital gain balancing: a new detection scheme for high-speed chemical species tomography of minor constituents

# Auto-Digital Gain Balancing: A New Detection Scheme for High-Speed Chemical Species Tomography of Minor Constituents

Sandip Pal* and Hugh McCann

School of Electrical & Electronic Engineering, University of Manchester, UK.

*Now at Variable Energy Cyclotron Centre, Bidhan Nagar, Kolkata, India.
E-mail: sandip@vecc.gov.in

**Abstract.** In many dynamic gas-phase reaction processes, there is great interest to measure the distribution of minor constituents, i.e. < $10^{-3}$ by volume (1000 ppm). One such case is the after-treatment of automotive gasoline engine exhaust by catalytic conversion, where a characteristic challenge is to image the distribution of 10 ppm (average) of carbon monoxide (CO) at 1000 frames per second across a 50 mm diameter exhaust pipe; this particular problem has been pursued as a case study. In this paper, we present a novel electronic scheme that achieves the required measurement of around $10^{-3}$ absorption with $10^{-4}$ precision at kHz bandwidth. This was not previously achievable with any known technology. We call the new scheme Auto-Digital Gain Balancing (Auto-DGB). It is amenable to replication for many simultaneous measurement channels, and it permits simultaneous measurement of multiple species, in some circumstances. Experimental demonstrations are presented in the near-IR. In single scans of a tunable diode laser, measurements of both CO and $CO_2$ have been achieved with 20 dB signal-to-noise ratio (SNR) at peak absorption. This work paves the way for chemical species tomography (CST) of minor constituents in many dynamic gas-phase systems.

**Keywords** Chemical, species, tomography, minor, infra-red, absorption, detection, low-noise, high-speed, Auto-Digital Gain Balancing

## 1. Introduction

High-speed Chemical Species Tomography (CST) has been demonstrated for hydrocarbon (HC) fuel mixing with air in various laboratory set-ups (Hindle *et al.*, 2001; Wright et al. 2005a; Terzija et al. 2008), and inside the combustion chamber of one cylinder of a multi-cylinder production engine (Wright et al. 2010). The HC fuel is present at concentrations of several per cent, at which level the use of the weak near-infrared absorption feature of large HC molecules at 1700nm is adequate for tomography. Moreover, the 1700nm absorption feature of such large HC molecules is very broad and un-structured, allowing the use of fixed-wavelength laser sources. Due to environmental, legislative and economic pressures on vehicle and fuel manufacturers (Stone, 1999), there is great interest to study the interaction of combustion exhaust constituents with catalytic after-treatment systems, the species of interest including unburned HC, $NO_x$ and CO. However, these are all present typically at minor concentrations, i.e. <1000 parts per million by volume (ppm). The understanding of converter effectiveness is hampered by lack of knowledge of the flow pattern and of the distribution of minor constituents before and after catalytic treatment (Schweich 1990; Koltsakis and Stamatelos 1997). The currently established technology for measurement of these species in automotive product R&D entails extractive sampling for subsequent analysis. This approach does not provide spatial resolution, although various developments (Sutela et al., 1999; Kayes and Hochgreb, 1996) have enabled intra-cycle temporal resolution. For a truly in-situ

tomographic imaging solution in a 50 mm diameter cross-section, with similar temporal resolution, it is necessary to use the much stronger fundamental absorption lines available in the mid-infrared. We have previously studied CO as a test case (Pal et al., 2008a) at an average concentration of 10 ppm over the exhaust cross-section, showing that:

(1) the critical properties of the light source are satisfied by Quantum Cascade Lasers (QCLs);
(2) commercially available mid-IR optics can provide a suitable CST system; but
(3) for adequate image reconstruction, we must improve upon previous single-pass spectroscopic absorption measurement technology, by an order of magnitude, to yield absorption precision of typically $2\text{x}10^{-4}$ for measurement of CO absorption of around $2\text{x}10^{-3}$ at 1kHz bandwidth.

This paper addresses (3) above and demonstrates a novel measurement technique, Auto-DGB, which satisfies the requirement, as suggested in (Pal et al., 2008b). Moreover, the new Auto-DGB technique demonstrated here has been designed for a multi-channel CST system, promising a realistic prospect of imaging such low concentrations at frame rates around 1,000 frames per second.

Several authors have studied sensitive spectroscopic measurement in the mid-IR, including measurement of NO, CO and other molecules. The Noise-Equivalent Sensitivity (NES) of such measurements is defined as the absorbance level that is equal to the noise level (i.e. SNR=1), divided by the square root of the measurement bandwidth, B, and it is given in units of absorbance per $(\text{Hz})^{½}$. For CO, the best previous NES performance is given as $5\text{x}10^{-6}$ per $(\text{Hz})^{½}$ with bandwidth 10 Hz, maximum among all (Wehe et al., 2003); requirement (3) above is equivalent to a NES value of $3\text{x}10^{-6}$ per $(\text{Hz})^{½}$, with bandwidth 1 kHz.

The noise sources of major concern in this type of spectroscopic measurement are gas baseline fluctuations, laser noise, detector noise, noise due to optical interference effects ("fringes"), electronic noise and electronic baseline drift (So et al. 2006). To achieve noise reduction, two measurement techniques have been most prominent in the literature: balanced ratiometric detection (BRD) and wavelength modulation spectroscopy (WMS). The BRD technique cancels laser intensity noise by using a two-beam approach, whereby one beam undergoes absorption in the measurement subject, and one is measured directly to provide a reference signal. BRD has been implemented in analogue form (Hobbs 1990, 1997, Allen et al. 1995, Sonnenfroh and Allen 1996, Sonnenfroh et al. 2001) and in digital form (Hafiz and Ozanyan 2007). The sensitivity is highest for nearly-balanced photocurrents, and the detection limit is shot-noise-limited, although it cannot eliminate phase noise effects (Hobbs 1997). Optical fringes can be a significant part of the measurement signal and ultimately limit the performance. BRD is severely bandwidth-limited, ultimately by the wavelength scan-rate of the source laser. Allen et al. (1995) and Sonnenfroh and Allen (1996) used BRD for sensitive detection in the visible and near-IR ranges, achieving NES 1.6 x $10^{-6}$ per $(\text{Hz})^{½}$ with bandwidth 0.1 Hz, as discussed in section 4.

Digital implementation of BRD (i.e. DBD) has been reported by Hafiz and Ozanyan (2007), digitizing the signal and reference voltages directly at the output of the preamplifiers. The reference signal, $V_R$, and absorption signal, $V_S$, are given by:

$$V_R(\nu,t) = F_R G I(\nu,t) + \Omega_R \tag{1}$$

$$V_S(\nu,t) = F_S G T(\nu,t) I(\nu,t) + \Omega_S \tag{2}$$

where,

$I(\nu,t)$ is the time-varying incident laser intensity and $\nu$ is the optical output frequency of the laser,
$F_R$ and $F_S$ are, respectively, the fraction of the laser output intensity that is directed along the reference and absorption paths,
$G$ is the optical-electrical gain of the detection system,
$T(\nu,t)$ is the transmission through the absorbing medium, and
$\Omega_R$ and $\Omega_S$ are offsets of the detection systems introduced by dark current, stray light falling on the detector, and the preamplifier.

DBD requires reference calibration to find the balancing factor BF=$F_S/F_R$ by removing the absorbing object. If the offsets are measured and subtracted from the measured voltages, then

$$T(\nu,t)=\frac{V_S(\nu,t)-\Omega_S}{V_R(\nu,t)-\Omega_R}\frac{1}{BF} \tag{3}$$

To avoid the requirement to measure offsets, Hafiz and Ozanyan (2007) introduced a modulated light source and used window-averaged mean differentials of the reference and the absorption signal, also helping to remove the phase dependence. They did not specify the measurement sensitivity achieved.

Tunable Diode Laser Absorption Spectroscopy (TDLAS) is the most commonly used technique for sensitive gas detection, and is based on scanning the laser output wavelength through an absorption feature of the target gas. This form of TDLAS is often referred to as Direct Absorption Spectroscopy (DAS), and is achieved by applying a current ramp to drive the laser. In light of the requirements of sensitive detection for minor species, DAS is incapable of reaching the required low detection limit due to various noise sources, but it allows all computations such as baseline fit and Voigt profile fit, if required. A major disadvantage of DAS is that the dynamic range of the analog-to-digital converter (ADC) is wasted on the sloping background and on the signal offset, if the absorption signal is small. It also requires interpolation of the background across the absorption feature, which is susceptible to errors from stray absorption and nonlinearity produced by the optical set-up. BRD has the advantage of dynamic balancing but its commercial analogue version is very expensive for use in multiple paths in a tomography system (Hafiz and Ozanyan 2007). Custom-made analogue versions require highly matched photodiodes and transistor pairs in the balancing circuitry for signal and reference, which is not essential in the digital case. Top of the range commercially available analogue balancing has a limited bandwidth of 125 kHz, and limited flexibility and performance (Hafiz and Ozanyan 2007). The DBD method introduced by Hafiz and Ozanyan (2007) is limited by balancing factor calibration as noted above, and it has similar limitations as for DAS, *viz.* decrease in dynamic range of the ADC. Wavelength-dependent optical effects that are not in common mode introduce significant error in measurement.

WMS is another form of TDLAS used for narrow absorption features, where modulation of the laser output power and wavelength is applied by modulating the laser driving current (with frequency f) . Detectability is improved by operating at sufficiently high frequency to effectively eliminate flicker (1/f) noise and by lowering the noise-bandwidth through lock-in detection. The WMS signal is dependent on the curvature of the spectral feature instead of the absolute absorption, and is less sensitive to variations in the incident laser intensity (Liu et al 2004). In WMS there is no simple resemblance of the demodulated signal (either at f or at 2f) to the absorption feature lineshape, and the optimal values of f and the modulation amplitude depend on the absorption feature. The background signal arises from laser non-linear intensity variation and interference fringes and the bandwidth is dependent on the cut-off frequency of the lock-in amplifier. An extensive review of WMS is given by Kluczynski (1999, 2001a, 2001b, 2001c). In general, the 2-f signal provides better sensitivity. The WMS characteristic is very much dependent on the absorption feature which is in turn dependent on pressure and temperature. Using 2-f WMS, Wang et al (2000a) achieved CO sensitivity of 0.1 ppm-m at 2.5 Hz bandwidth, equivalent to NES $1.3\text{x}10^{-6}$ per $(\text{Hz})^{½}$. This technique requires a wide wavelength scan of the laser to include the entire spectrum of the absorption feature. Being complex, it requires a great deal of memory and computation capacity for multi-path implementation. Dynamic calibration and optimization of the instrument parameters are also very difficult to implement.

In summary, none of the previously established techniques is able to achieve sensitive detection, high bandwidth and tomographic application. In this paper, the novel technique of Auto-DGB is proposed, based on a new form of balancing implemented in the digital domain. It is equally applicable both for operation with dc laser current drive, and dc with ac modulation of the laser current. The principle and mathematical analysis of Auto-DGB, and a thorough simulation of its performance, are presented in Section 2. In Section 3, an experimental demonstration of the new technique is reported. Discussion and comparison with other authors are presented in Section 4, and conclusions are given in Section 5.

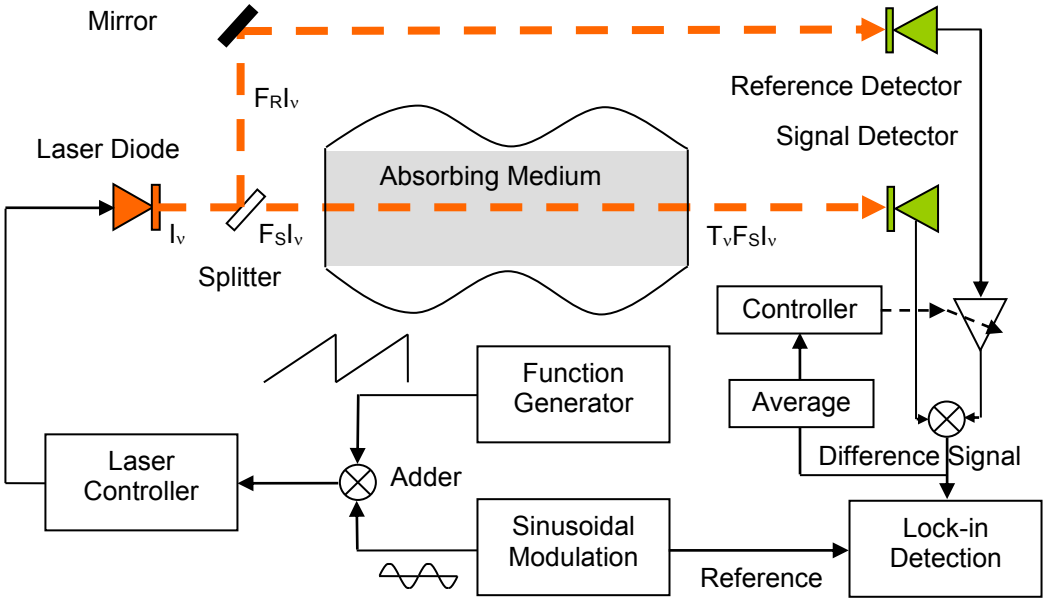


**Figure 1: Schematic diagram of the Auto-DGB technique**

## 2. Auto-Digital Gain Balancing

*2.1. Principle*

Figure 1 shows a schematic diagram of the principle of Auto-DGB. The resulting voltage signal of the reference channel is amplified or attenuated using an amplifier with gain selected by a controller with a negative feedback in such a way that the difference output of the two channels becomes zero. Therefore, the absorption signal is encoded within the gain when balance is achieved, i.e. the "balance gain". The ratio of the balance gain at the peak wavelength of the absorption feature to that at the wings (i.e. without any absorption by the species of interest) provides the exact transmission factor. The same circuit can be implemented both with dc optical intensity as well as an ac modulated signal. In the latter case, the moving average of the difference signal is fed back to the controller, and a lock-in amplifier is applied to the difference signal to implement WMS.

*2.2. Mathematical analysis*

To model Auto-DGB, equations (1) and (2) are modified by introducing laser noise, $e(t)$, as an additive component to the laser intensity. For transmission through combustion exhaust (neglecting nitrogen):

$$V_R(\nu,t) = F_R G\left[I(\nu,t) + e(t)\right] + \Omega_R \tag{4}$$

$$V_S(\nu,t) = F_S G T_{CO}(\nu,t) T_{CO_2}(\nu,t) T_{H_2O}(\nu,t)\left[I(\nu,t) + e(t)\right] + \Omega_S \tag{5}$$

where the total transmission factor, $T(\nu,t)$ in equs. (2) and (3), is split into multiplicative components for each of the species CO, $CO_2$ and $H_2O$. If offsets $\Omega_R$ and $\Omega_S$ are measured separately and subtracted, then the difference voltage $V_D$ can be formed, taking account of the gain factor, $\Xi(\nu,t)$, applied to $V_R$, as follows:

$$V_D(\nu,t) = \Xi(\nu,t)\left[V_R(\nu,t) - \Omega_R\right] - \left[V_S(\nu,t) - \Omega_S\right] \tag{6}$$

By varying $\Xi(\nu,t)$ to achieve balance, i.e. $V_D(\nu,t) = 0$, then, analogous to equation (3), we obtain:

$$\Xi(\nu,t) = \frac{V_S(\nu,t) - \Omega_S}{V_R(\nu,t) - \Omega_R} = \frac{F_S}{F_R} T_{CO}(\nu,t) T_{CO_2}(\nu,t) T_{H_2O}(\nu,t) \tag{7}$$

The ratio $F_S/F_R$ = BF appears, as in equation (3). In Auto-DGB, however, BF can be eliminated by taking the ratio of the balance gains at two different optical frequencies, $\nu_1$ and $\nu_2$:

$$\frac{\Xi(\nu_1,t)}{\Xi(\nu_2,t)} = \frac{T_{CO}(\nu_1,t) T_{CO_2}(\nu_1,t) T_{H_2O}(\nu_1,t)}{T_{CO}(\nu_2,t) T_{CO_2}(\nu_2,t) T_{H_2O}(\nu_2,t)} \tag{8}$$

In TDLAS, the optical frequency scan is performed in about 1 ms, during which the exhaust composition can be assumed constant and the transmission of each constituent will only depend on ν, thus yielding:

$$\frac{\Xi(\nu_1)}{\Xi(\nu_2)} = \frac{T_{CO}(\nu_1)T_{CO_2}(\nu_1)T_{H_2O}(\nu_1)}{T_{CO}(\nu_2)T_{CO_2}(\nu_2)T_{H_2O}(\nu_2)} \tag{9}$$

If $\nu_1$ is chosen to be at the peak absorption point of the selected absorption feature of CO, and $\nu_2$ at the wing of the absorption line, i.e. $T_{CO}(\nu_2) = 1$, and if the transmission values for $CO_2$ and $H_2O$ are the same at both $\nu_1$ and $\nu_2$ , then the balance gain ratio is the transmission value of CO at $\nu_1$, since equation (9) becomes:

$$T_{CO}(\nu_1) = \frac{\Xi(\nu_1)}{\Xi(\nu_2)} \tag{10}$$

Even in the case where absorption due to $CO_2$ and $H_2O$ are significant, one can still isolate and measure absorption due to CO. Just as in BRD, the laser noise is removed, but BF is eliminated. This has been made possible by fast adjustment of the gain (Ξ) to balance the difference voltage $V_D$ to zero. Hence, the method is named Auto-Digital Gain Balancing.

*2.3. Implementation with WMS and PSD*

In conjunction with Auto-DGB it is possible to apply WMS and Phase Sensitive Detection (PSD). To achieve PSD (often called "lock-in detection"), a suitable sinusoidal modulation of the laser source is applied at a high frequency, f; typically, the resultant absorption signal is then multiplied by the modulation signal and/or its harmonic at 2f, both in phase and in quadrature, and the dc component is then selected by a filter, to yield both the magnitude and phase difference of the sinusoids, including the effects of the absorption features. The lock-in detection scheme of the difference signal of the Auto-DGB technique is shown in Figure 1. The theory of WMS in Auto-DGB can be found in Pal (2009). The drive current of the laser diode has two components – a dc component and an ac modulation component. The laser frequency $\nu(t)$, in $cm^{-1}$, varies in the same manner as the current and it is assumed that the frequency modulation (FM) amplitude is linearly related to the current modulation amplitude. The variation of the laser intensity is considered nonlinear with respect to the injection current (Kluczynski et al. 2001a and Li et al. 2006) and is given by

$$I_L(\nu_c, \nu_a, t) = I_{L,0}(\nu_c)\left[1 + i_{L,1}(\nu_a)\cos(2\pi ft + \psi_1) + i_{L,2}(\nu_a)\cos(2\pi 2ft + \psi_2)\right] \tag{11}$$

where $I_{L,0}(\nu_c)$ is the laser centre power, $i_{L,1}$ and $i_{L,2}$ are the linear (1f) and nonlinear (2f) intensity modulation (IM) amplitudes normalised to $I_{L,0}(\nu_c)$, respectively, $\psi_1$ is the FM/IM phase shift, and $\psi_2$ is the phase shift of the nonlinear IM with respect to FM. Typical characteristics of the Specdilas laser (from datasheet) used in the experimental work discussed in section 3 below are best-fitted to the equation $I_{L,0}(\nu_c) = -0.0304 \cdot \nu_c^2 + 383.69 \cdot \nu_c - 1212596.5$ mW.

The $k$-th harmonic of the output signal of the lock-in amplifier $S_k(\nu_c, \nu_a)$ is mathematically analogous to the $k$-th Fourier component of the time-dependent photodiode signal. For 2-f detection, the photodiode signal is multiplied with a sinusoidal reference signal $\cos(2\pi 2ft - \theta_k)$. The spectral absorbance, $\alpha(\nu)$ is a periodic even function of $2\pi ft$ (Li et al. 2006) and can be expanded as a Fourier cosine series given by:

$$-\int_0^L \sum k_\nu(x)dx = -\alpha(\nu_c + \nu_a\cos(2\pi ft)) = \sum_{k=0}^{\infty} H_k(\nu_c, \nu_a)\cos(2\pi kft) \tag{12}$$

where $H_k$ is the corresponding set of Fourier coefficients. For optically thin samples, $\alpha(\nu) \ll 1$, the fractional transmission of a monochromatic signal, $T_\nu$ according to the Beer Lambert Law and assuming no scattering, is given by:

$$S(\nu_c, \nu_a, t) = I_L(\nu_c, \nu_a, t) * T_\nu = I_L(\nu_c, \nu_a, t) * e^{-\alpha(\nu)} \approx I_L(\nu_c, \nu_a, t) * \left(1 - \alpha(\nu)\right) \tag{13}$$

The output signal of the 1-f and 2-f lock-ins, in-phase and quadrature, have been given by (Li et al. 2006). The 2-f signal is dependent on five Fourier components ($H_0$, $H_1$, $H_2$, $H_3$, $H_4$) and two phase shifts, $\psi_1$ and $\psi_2$, due to the nonlinear amplitude of IM, $i_{L,2}$. Though the value of $i_{L,2}$ is small, its contribution to the 2-f output signal is comparable to the absorption-based signal in the case of absorption by a minor species over a short pathlength. The dependence on $H_0$ and $H_4$ can be eliminated if $i_{L,2}=0$. It is possible to isolate

the Residual Amplitude Modulation (RAM), i.e. the signal due to the nonlinear term of the laser intensity modulation, for the case where there is no absorption. It is evident that RAM makes a significant contribution when sensitive measurement is desired.

Although some phase difference, $\Delta\psi$, will be introduced between the two channels by the electronics and and the phase delay of the control loop, for the sake of simplicity it is assumed that $\Delta\psi = 0$, giving:

$$V_R(\nu_c,\nu_a,t) = F_R G I_L(\nu_c,\nu_a,t) + \Omega_R \tag{14}$$

$$V_S(\nu_c,\nu_a,t) = F_S G I_L(\nu_c,\nu_a,t) T(\nu_c,\nu_a,t) + \Omega_S \tag{15}$$

The moving average of these signals for an integral number of periods of the modulation frequency produces the following equations, where the cosine terms vanish:

$$\bar{V}_R(\nu_c) = F_R G I_{L.0}(\nu_c) + \Omega_R \tag{16}$$

$$\begin{aligned}\bar{V}_S(\nu_c,\nu_a) &= F_S G I_{L.0}(\nu_c)\left(1 - \overline{\alpha(\nu_c + \nu_a\cos(2\pi ft))}\right) + \Omega_S \\ &= F_S G I_{L.0}(\nu_c)\left(1 + H_0(\nu_c,\nu_a)\right) + \Omega_S\end{aligned} \tag{17}$$

where $\overline{\alpha(\nu_c,\nu_a)}$ is the average value of absorbance, $\alpha(\nu_c,\nu_a)$. From equ. (12), $\overline{\alpha(\nu_c,\nu_a)}$ is replaced by the fundamental Fourier coefficient. From equ. (7), and using equs. (16) and (17), we obtain:

$$\Xi(\nu_c,\nu_a) = \frac{\bar{V}_S(\nu_c,\nu_a) - \Omega_S}{\bar{V}_R(\nu_c) - \Omega_R} = \frac{F_S}{F_R}\left(1 + H_0(\nu_c,\nu_a)\right) \tag{18}$$

The instantaneous difference signal from (14) and (15), via equ. (6), and using $\Xi$ from equ.(18), is:

$$\begin{aligned}V_D(\nu_c,\nu_a,t) &= \Xi(\nu_c,\nu_a)\left(V_R(\nu_c,\nu_a,t) - \Omega_R\right) - \left(V_S(\nu_c,\nu_a,t) - \Omega_S\right) \\ &= \left\{F_S G I_L(\nu_c,\nu_a,t)\right\}\left[\left(1 + H_0(\nu_c,\nu_a)\right) - T(\nu_c,\nu_a,t)\right]\end{aligned} \tag{19}$$

Assuming $\Delta\psi = 0$, then replacing $T$ from equ. (13) yields:

$$V_D(\nu_c,\nu_a,t) = -F_S G I_{L,0}(\nu_c,\nu_a,t)\sum_{k=1}^{\infty} H_k(\nu_c,\nu_a)\cos(2\pi kft) \tag{20}$$

Comparing equs. (12) and (20), the 2-f lock-in signal will be obtained by eliminating the term $\left(1 + H_0(\nu_c,\nu_a)\right)$. The 2-f component of the difference signal from PSD is given by:

$$V_{D,2f}^{even} = -\frac{F_S G I_{L,0}}{2}\left[H_2 + \frac{i_{L,1}}{2}(H_1 + H_3)\cos\psi_{1,R} + i_{L,2}\frac{H_4}{2}\cos\psi_{2,R}\right] \tag{21}$$

$$V_{D,2f}^{odd} = \frac{F_S G I_{L,0}}{2}\left[\frac{i_{L,1}}{2}(H_1 - H_3)\sin\psi_{1,R} - i_{L,2}\frac{H_4}{2}\sin\psi_{2,R}\right] \tag{22}$$

where $\psi_{1,R}$ and $\psi_{2,R}$ are the corresponding phase shifts to $\psi_1$ and $\psi_2$ for the reference and absorption signal.

The absolute magnitude of the 2-f signal is given by:

$$V_{D,2f} = \sqrt{(V_{D,2f}^{even})^2 + (V_{D,2f}^{odd})^2} \tag{23}$$

If equs. (21) and (22) are compared with the conventional WMS signals (Li et al. 2006), then it is found that:

(i) There is no RAM signal present in the Auto-DGB output;

(ii) Since the nonlinear IM term $i_{L,2}$ is very small and the $(1+H_0)$ term is not present in the coefficient of the $i_{L,2}$ term as compared to general 2f-WMS, $H_4$ dependency can be neglected and the asymmetry terms are only dependent on $H_1$ and $H_3$, odd terms of the absorption. Since $H_1$ and $H_3$ are zero at the peak absorption frequency, the peak absorption will be unaffected.

(iii) The peak value of the demodulated 2-f signal varies with the laser intensity, which can be eliminated after normalisation with 1-f signal (Li et al. 2006). The same can be achieved even for the difference signal of Auto-DGB.

As described earlier, the dependence on the offsets can be eliminated by measuring them separately and subtracting $\left(\Xi(\nu_c,\nu_a)\Omega_R-\Omega_S\right)$ from the difference signal. At every instant of time, the measured Ξ at the previous instant is used to evaluate the offset term. If the difference signals are measured with different known attenuation factors while keeping the laser drive current below threshold, then:

$$V_{O,1}=\Xi_1\Omega_R-\Omega_S \tag{24a}$$

$$V_{O,2}=\Xi_2\Omega_R-\Omega_S \tag{24b}$$

Solving equs. (24a) and (24b), we obtain:

$$\Omega_R=\frac{V_{O,1}-V_{O,2}}{\Xi_1-\Xi_2} \quad \text{and} \quad \Omega_S=\frac{\Xi_2V_{O,1}-\Xi_1V_{O,2}}{\Xi_1-\Xi_2} \tag{25}$$

The above sequence of operations is shown schematically in figure 2.

*2.4. Simulation*

Auto-DGB has been simulated using Simulink where several components were implemented as shown in figure 2, using measured characteristics of appropriate laser sources (intensity and wavelength vs. injection current). The laser linewidth (FWHM) was set to 0.00033 $cm^{-1}$ (10 MHz) for both the spectroscopic DFB laser Specdilas-D (used in Near-IR experiments below) and a CW QCL (for mid-IR). A Lorentzian distribution of the laser power was assumed at the centre optical frequency. The laser central frequency was scanned over the entire spectral range in 1 ms.

Two types of scheme were tried, one with a smooth ramp scan of laser frequency, and another with discrete steps. Since the ramp signal is dynamic, its performance is based on the time delay from the PI (Proportional Integral) controller, the averaging process and the low pass filter. Hence, a perfect match of their characteristics is required in order to reduce artefacts. For the discrete step approach, if a sufficient period of time is allowed in every step, then actual readings would be expected in each step without the delay introduced by other parts of the circuit. These two different simulation results are required to match each other for validating the performance of all other components. For near-IR the current scan was 40 mA and for mid-IR the scan was 120 mA to cover the desired absorption spectral ranges.

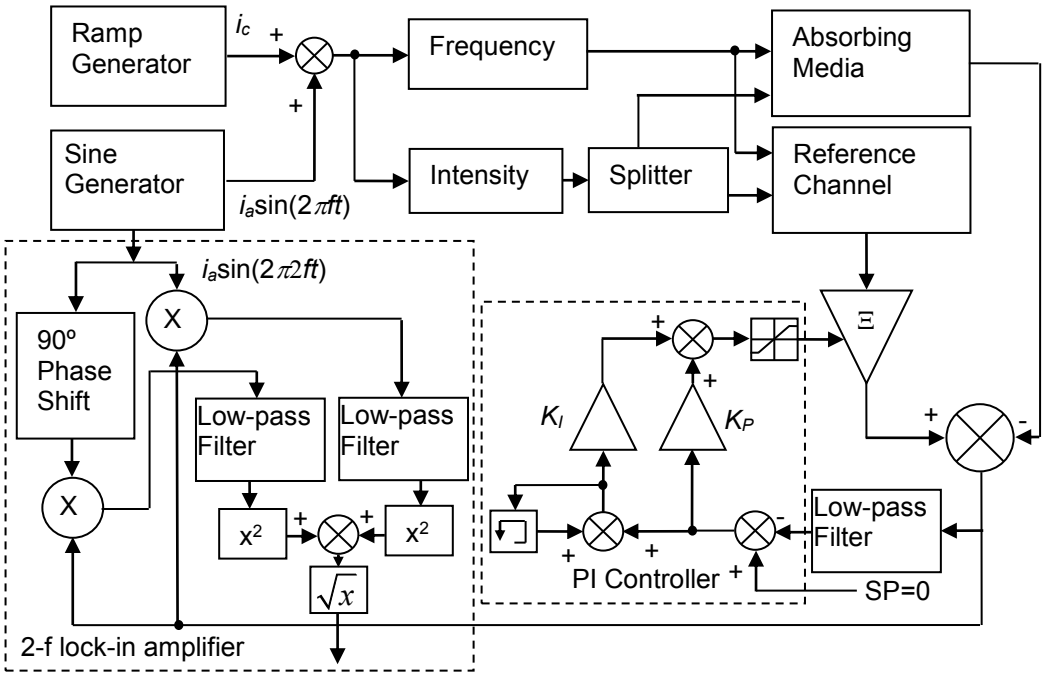


**Figure 2: Schematic diagram of Auto-DGB for simulation**

For implementation of the 2f-WMS technique, a modulation sinusoid of different amplitude was added to the centre frequency ramp scan. In both cases – normal Auto-DGB and Auto-DGB with 2f-WMS - the

difference signal between the attenuated reference signal and the absorption signal is averaged over integral multiples of the period of the modulation waveform. This difference is used as the feedback signal, which is then free from the modulated signal. A PI controller takes this feedback signal as measurement input and tries to set it to zero, i.e. the setpoint is zero, as shown in figure 2. The PI controller varies the gain of the reference channel so that the dc part of the difference signal is zero. The integral term (I) of the controller is implemented in digital format by adding the errors (setpoint - input signal) together and multiplying with an integral constant. A saturation function is added after the adder of the P (proportional) and I terms so that there is a maximum or minimum value in case this term exceeds the saturation value. Normal Auto-DGB is obtained from the ratio of the gains at the peak absorption wavelength and at the wing of the absorption feature.

In 2f-WMS, a PSD scheme was implemented on the difference signal, $V_D$, to get the 2-f signal. After multiplying $V_D$ with the cosine and sine of twice the modulation frequency, a low-pass filter was implemented by a moving-window average for a length of signal equivalent to an integral multiple of the modulation time period so that the modulation frequency term and its harmonics would be eliminated. Therefore, the dc signal outputs after filtration was the in-phase and quadrature terms of 2f-WMS.

Simulation has been performed for two CO absorption regions, about 2169.5 $cm^{-1}$ in the mid-IR and about 6330.5 $cm^{-1}$ in the near-IR (Rothman, 1996, 2005; Pal et al., 2008a), to evaluate the performance of the electronic scheme. In both cases, the laser linewidth was convoluted with the absorption feature. For brevity, only the mid-IR simulation results are presented in this sub-section. As shown in Figure 3(a), the laser frequency $\nu_1$ was scanned in steps of 0.02 $cm^{-1}$ through the R(6) absorption feature of CO; in between every step change of $\nu_1$, the current was set to a value that shifts the diode laser optical output to $\nu_2$, fixed at 2169.5926 $cm^{-1}$, where the absorption due to $CO_2$ and $H_2O$ is the same as that at the peak of the R(6) transition (Pal et al. 2008b). Sinusoidal modulation was not applied.

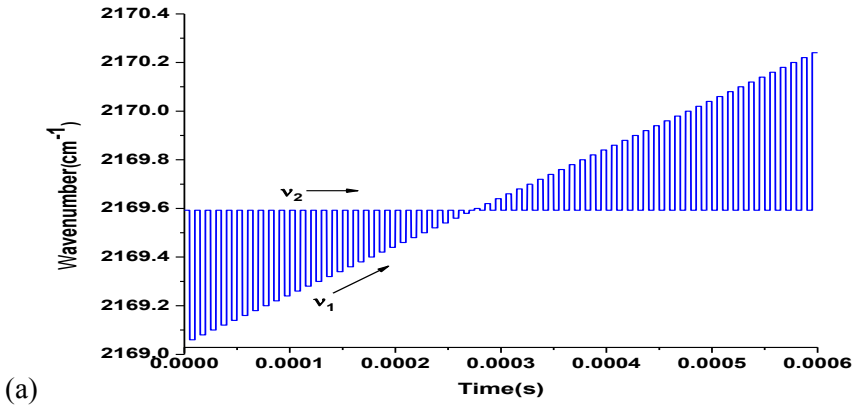


(a)

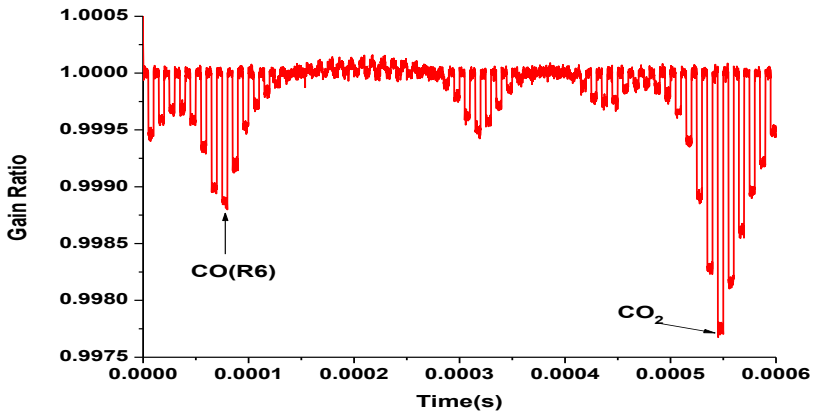


(b)

**Figure 3: Simulation of the Auto-DGB scheme: (a) the scanning and reference steps as a function of time, with a reference wavenumber of 2169.596 $cm^{-1}$; (b) the gain ratio output at every step of wavenumber.**

The absorption is measured at $\nu_1$ via the balance gain $\Xi(\nu_1)$; it is then measured at the reference wavelength, $\nu_2$, to obtain $\Xi(\nu_2)$. The waveform in Figure 3(b) (subject to noise, as discussed below) shows, for each step of $\nu_1$, the ratio of balance gain values between $\nu_1$ and $\nu_2$. Thus, the effect of absorption baseline is removed dynamically via eqn. (9). Figure 3(b) shows that the peak CO absorption is reached at 2169.2 $cm^{-1}$. The simulated full scan took around 0.6 ms for a total scan of about 1.25 $cm^{-1}$. This demonstrates that the Auto-DGB scheme achieves a spectral absorption measurement. Another peak is observed at 2170.2 $cm^{-1}$ which is due to $CO_2$. In this way, Auto-DGB can measure multiple species present in the sample. In the simulation, a random band-limited noise of flat power spectral density (PSD) $10^{-11}$W/Hz has been added both for the common-mode as well as the individual channels with a sampling time of 0.1μs. These noise characteristics then show up in the noise level of the gain ratio in figure 3(b). Common mode noise is cancelled totally in this technique. Therefore, by selecting electronic components that yield low individual channel (uncorrelated) noise, and by selecting components with good discrimination in setting the gain values of the Auto-DGB scheme, it is clear from figure 3 that excellent SNR of absorption measurement is promised. Similarly, if two lines of a single species are scanned, e.g. $CO_2$, then the temperature of the sample gas can be estimated (Liu 2006).

Extensive simulations were performed in the near-IR region. The laser frequency range was scanned by using a ramp current, with and without fast sinusoidal modulation. In this case, the low pass filters are realised by a 256-sample moving average, i.e. four cycles for 156.25 KHz modulation and 10 MS/s sampling rate. The simulation investigated the effect of modulation amplitude and other parameters, e.g. the effect of averaging, the integral action of the controller and the low pass filter, and the laser linewidth. The combination of these effects is called the instrument function, and it convolves with the absorption feature lineshape to reduce the absorption peak. Modulation amplitude 2mA (~0.02 $cm^{-1}$) was found to maximize the 2-f WMS signal under conditions relevant to the experimental tests in Section 3.

The simulations confirmed that Auto-DGB has the following benefits for minor species applications:

- Common-mode optoelectronic noise effects (additive and multiplicative) are eliminated, as are baseline fluctuations and the sloping background of intensity.
- It eliminates the calibration requirement for the balance factor.
- It eliminates the need for RAM measurement.
- The method is reconfigurable and versatile, enabling optimization of modulation conditions.
- Electronic offsets, and offsets arising from stray light, can be eliminated.
- The dynamic range of the measurement is enhanced in an iterative manner by amplification as the difference signal is measured and zeroed during the PI process.

## 3. Implementation and Demonstration of Auto-DGB

### *3.1. Experimental set-up*

The first demonstration of Auto-DGB was carried out in the near-IR, since the demands of the optical set-up are much simpler than for the mid-IR. The absorption strengths are orders of magnitude lower than in the mid-IR, but this can be overcome by using higher concentrations of the target species. A near-IR laser diode (Specdilas D type) was mounted on a laser mount TCLD-M9, equipped with a temperature sensor (AD 590) and a Thermo-Electric Cooler (TEC). The TEC and diode injection current were driven by a Thorlabs laser controller (ITC510). The overall arrangement is shown in figure 4. The beam was launched with a collimating lens (Thorlabs C240TME-C) with 8 mm focal length and 0.5 numerical aperture (NA). InGaAs PIN photodiodes were used (Hamamatsu G8370-81).

Optical alignment is critical for perfect balance so that the baseline of the Auto-DGB measurement is constant throughout the scan, and was achieved by maximizing the detector signal whilst the alignment was adjusted. The laser source was extensively calibrated (Pal, 2009). Two modes of Auto-DGB were tested, one with a current ramp and no fast modulation, and the other with a 156.25 kHz sinusoidal modulation superimposed on the current ramp. Both of these were superimposed on a dc current of about 74 mA set by the laser driver to maintain the laser diode above threshold. The 1ms current ramp scanned the laser output wavelength over a range of 0.3 nm (~1.2 $cm^{-1}$). The modulation amplitude was set at 2.5 mA, driven by an 11-bit Direct Digital Synthesiser (DDS), as discussed in sub-section 2.3.

*3.2. Electronics*

Figure 5 shows the electronic scheme to implement Auto-DGB. The laser source is driven by signals generated by a DDS coded on the Field Programmable Gate Array (FPGA). Each photodetector feeds into a variant of the low-noise transimpedance amplifier of Wright et al. (2005b). The reference signal is amplified using a multiplying Digital-to-Analog Convertor (MDAC) to achieve zero difference signal

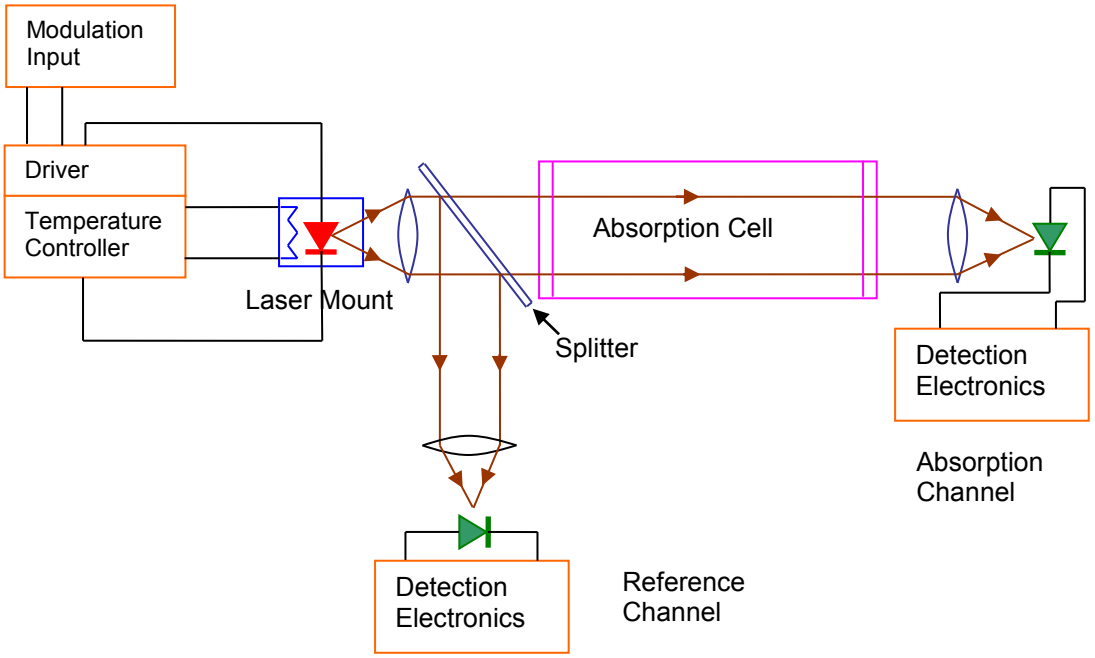


**Figure 4: Schematic view of the experimental set-up for the ADGB demonstration.**

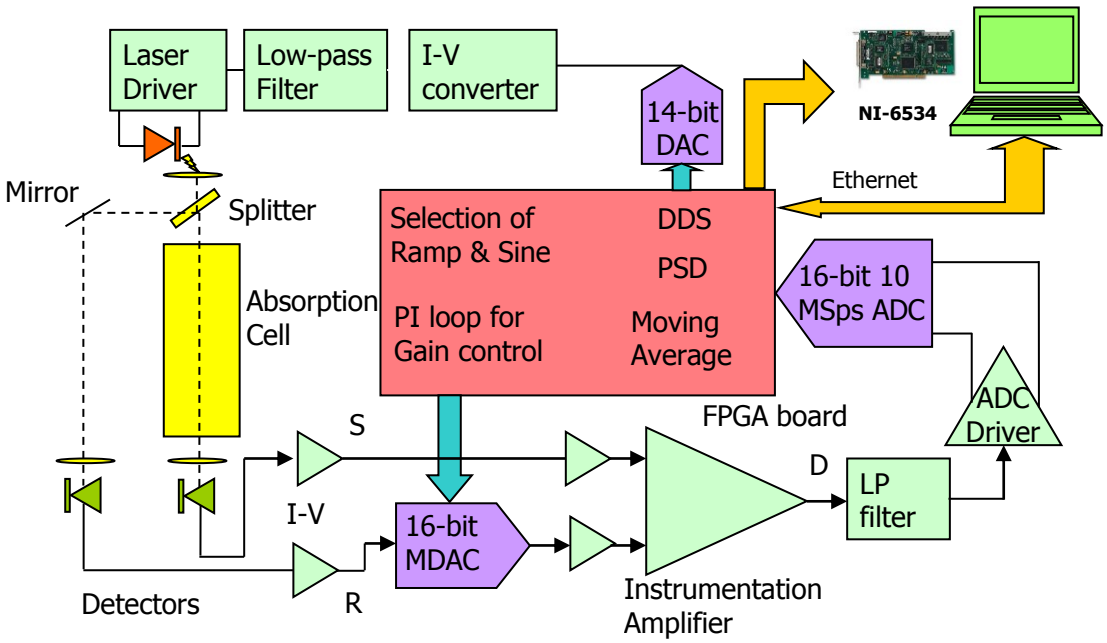


**Figure 5: Schematic view of electronic implementation of the Auto-DGB technique.**

(with respect to the absorbed signal) at the output of the downstream instrumentation amplifier. The amplified difference signal is digitized by an ADC ADS1610 and then stored in the FPGA for processing, including moving-average filtering and PI control, as discussed in sub-section 2.4, to generate a control signal, which is an MDAC gain code. The reference signal amplitude is maintained at twice that of the absorbed signal so that the MDAC is in the middle of its range. Therefore, the transmission signal is encoded in the MDAC gain but amplified with the digital range of the MDAC and the splitting ratio $F_S/F_R$ (see equ. (7)). The amplification term is eliminated by ratioing the MDAC gain code at different laser

frequencies as discussed in sub-section 2.3 (see equ. (9)). The drift and dc errors can be eliminated by measuring the zero-absorption signals and applying equ. (18) periodically.

The stability and settling time of the control loop are important and are set by proper selection of the proportional gain and integral constant of the PI controller. The stored signal in the FPGA can be processed for 1-f or 2-f PSD, as in WMS. We note that Barrass et al. (2004) and Zhu and Cassidy (1995) reported systems which applied WMS to the difference output of an analogue BRD instrument.

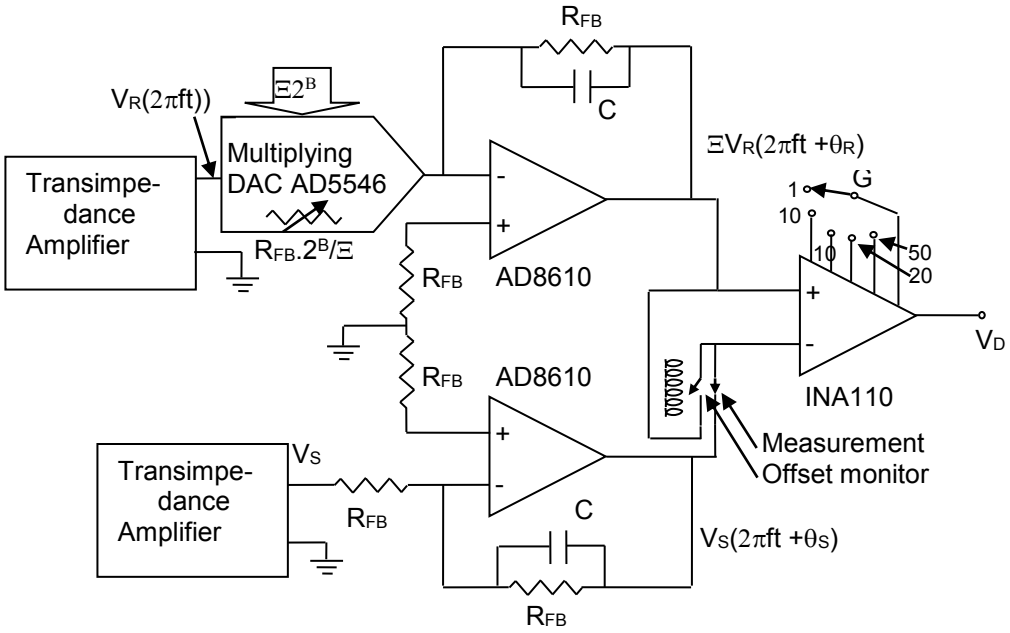


**Figure 6: Schematic diagram of the balancing circuit**

The balancing circuit, shown in Figure 6, is the main component of the Auto-DGB technique. The 16-bit MDAC (AD5546) is of parallel-input, current-output design, and its output is converted to voltage by an I-to-V converter with feedback resistance, $R_{FB}$, that is internally matched for minimum gain error. The FET-input op-amp AD8610 is chosen for this purpose, for its high input impedance and great precision. The AD8610's input offset voltage is multiplied by the variable noise gain arising due to the code-dependent output resistance of the MDAC. There will be a step change in the output voltage if the noise gain changes between two adjacent digital inputs, requiring that the input offset voltage of the op-amp should be a fraction of the LSB of the DAC. The AD8610/8620 has very low bias current of 2pA and offset voltage of 45 μV at 25º C (Analog Devices datasheet). Though the offset voltage is equivalent to 1 LSB of DAC input, the AD8610/8620 is chosen for its ultralow-noise performance. Output voltage noise is dominated by $R_{FB}$. A detailed noise analysis for the MDAC is available in an application report (Noxon, 2006). The non-linearity error has a maximum value ±2 LSB, but for very small change of digital codes, it generates linearity error of ±0.2 LSB. In the experiments reported here, the code change is very small as the absorption level is very low. If the gain error for the internally matched feedback resistor is considered zero, the gain error at the output is dependent only on the non-linearity error which is equivalent to an absorption value of $\pm 3.10^{-5}$ for ±0.2 LSB.

A compensation capacitor of 10 pF is added in parallel to $R_{FB}$ to smooth the current signal when the MDAC code changes, to avoid gain peaking and ringing at the I-to-V converter output. The digital input of the MDAC is updated at 10 MHz for feedback control so that the two channels balance each other, yielding zero dc output. The multiplying bandwidth is 4 MHz for attenuation level within -36 dB for unipolar operation. Since the change in signal for subsequent digital inputs is low, the update rate of 10 MHz is very well maintained. To balance the phase in the absorption channel also, another AD8610 is used. The outputs of the AD8610s are fed to the fast-settling INA110, with a gain set at 100 so that the -3dB bandwidth (470 kHz) was comfortably greater than twice the modulation frequency. Input bias and offset currents are 20 and 2 pA, respectively, and they are measured at regular intervals by using the relay

at the input of the INA110, and subtracted dynamically in the rest of the cycle during actual measurement. For stable PID output, a low-pass filter was used (-3dB at 341 kHz).

*3.2. Experimental demonstrations*

The ultimate validation of Auto-DGB is to measure the known concentrations of target gases, in mixtures with known concentrations of other constituents. Three experiments were performed: two with reference gas cells 150mm long, at pressures of 200 torr $CO_2$ in one case and 600 torr CO in the other, and the third with a custom-built absorption cell filled with 20% CO, 24% $CO_2$ and 56% $N_2$ at atmospheric pressure. The results presented below are for one absorption line each for $CO_2$ (6330.818 $cm^{-1}$) and CO (6330.163 $cm^{-1}$). The reference optical frequencies used in the Auto-DGB process for the three experiments are 6330.41 $cm^{-1}$, 6329.6 $cm^{-1}$ and 6331.0 $cm^{-1}$, respectively, and chosen to be in the absorption baseline in each case. Where applied, sinusoidal modulation was at 156.25 kHz, with current amplitude 2.5 mA. Experimental measurements are compared with (a) calculations based on spectroscopy using the HITRAN database (Rothman et al. 1996, 2005), incorporating temperature, pressure, line broadening, etc., and (b) the effects of the instrument function, using the simulation procedure described in sub-section 2.4, incorporating the spectroscopic calculations. In all cases, measurement precision of the peak absorption is assessed by calculating its standard deviation for a randomly selected set of 100 consecutive scans.

*3.2.1. $CO_2$ without sinusoidal modulation.* Figure 7 shows the Auto-DGB measurement of the $CO_2$ absorption line, with peak absorption of 0.0123 relative to transmission of almost 1 at the extremes of the scan range. It also shows a number of local maxima in the wings of the peak absorption, which are measurement artefacts. The expected absorption profile, with and without the instrument function, is included. The peak of the measured absorption is about 71% of that calculated from the spectral database alone, i.e. case (a) above; this is to be compared with 82% when the instrument function is included, i.e. case (b) above. In the latter case, there is good agreement between measurement and simulation concerning the laser frequency position of peak absorption, whereas the measured position is shifted slightly relative to the purely spectral calculation. The shift is an artefact due to the PI controller behaviour. The standard deviation of peak measured absorption is 0.000156.

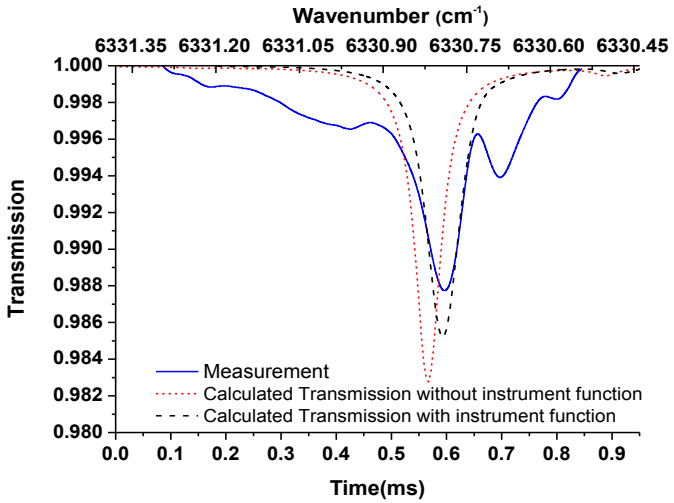


**Figure 7: Auto-DGB transmission measurement for $CO_2$ using a current ramp, compared with the calculated result from the spectroscopic database, with and without the instrument function.**

*3.2.2. $CO_2$ with sinusoidal modulation.* The Auto-DGB measurement yields peak absorption value 0.0120, agreeing well with the result found in 3.2.1. Measurement artefacts are reduced, compared to those in 3.2.1, because averaging of both WM and IM signals at feedback reduces the steepness of the control input. The standard deviation at peak absorption is 0.000128. The 2-f PSD process was applied to the difference signal of the Auto-DGB technique but no improvement in precision was observed.

*3.2.3. CO without sinusoidal modulation*. Figure 8 shows the measured transmission scan through the CO absorption line. The peak absorption in this case is 0.0210, i.e. 88% of that calculated in case (a) above, and 92% in case (b). The oscillations observed at the lower optical frequency region of the scan range are less dominant compared to $CO_2$ because the CO line at 600 torr is wider than the $CO_2$ line at 200 torr. The 100 consecutive scans from a randomly selected period are shown, overlaid, in Figure 9. They yield a standard deviation of 0.00011 for the peak absorption.

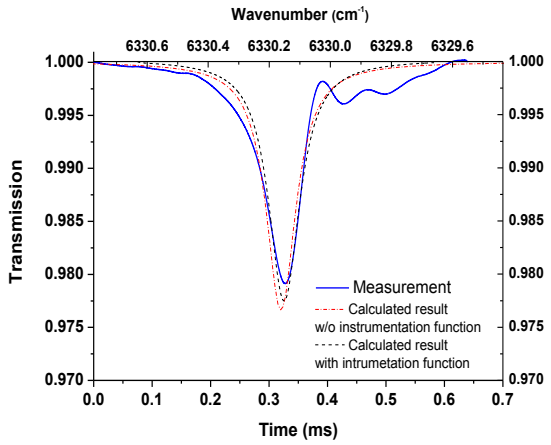


**Figure 8: Auto-DGB transmission measurement for CO using a current ramp, compared with the expected result calculated from the spectroscopic database, with and without the instrument function.**

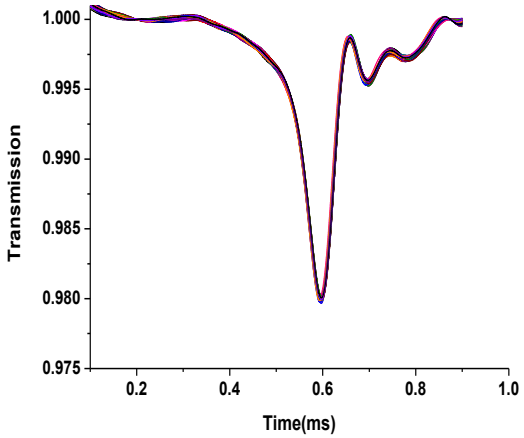


**Figure 9: One hundred consecutive Auto-DGB scans of CO absorption, superimposed.**

*3.2.4. CO with sinusoidal modulation.* In this case, the peak value of the absorption is 0.0183 which is 78% of that from calculation (a). As observed for $CO_2$, the sinusoidal modulation decreases the measurement artefacts. The peak absorption value was found to have a standard deviation of 0.00014. The 2-f PSD technique was also applied, but the result obtained was no more precise.

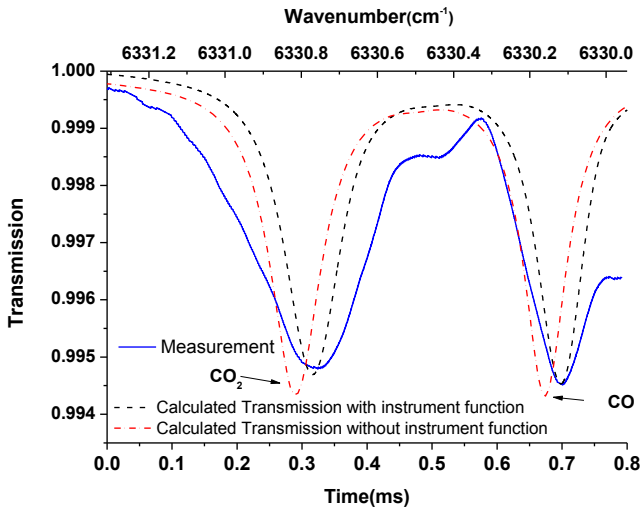


**Figure 10: Auto-DGB transmission measurement for 20% CO, 24% $CO_2$ and 56% $N_2$ (164 mm cell and 1.2 bar pressure at 296 K) using a current ramp, compared with the expected result calculated from the spectroscopic database, with and without the instrument function.**

*3.2.5. 20% CO, 24% $CO_2$ and 56% $N_2$, without sinusoidal modulation*. Interference fringes obtained with this absorption cell were minimised by aligning the beam off-axis with respect to the cell. Figure 10

shows a single Auto-DGB transmission scan through both of the chosen absorption features of CO and $CO_2$. The CO and $CO_2$ absorption peaks are clearly resolved in the same 1ms scan.

The peak absorption measurements are 0.0052 and 0.0055 for $CO_2$ and CO respectively, which are 90% and 95%, respectively, of the calculated values from case (a), reflecting the different linewidths. Incorporating the instrument function results in an almost perfect match between simulated peak absorbance and the measured value. The standard deviations calculated for the two peaks of $CO_2$ and CO are 0.000161 and 0.000215, respectively. In terms of relative precision, these results are better than the target level by a factor of about 3, which is equal to the increased path length in the experiment, relative to the target application. The standard deviation for the $CO_2$ peak is the same as that obtained in sub-section 3.2.1. The standard deviation for the CO peak is higher than that obtained in sub-section 3.2.3; the reason may be the relatively smaller absorption peak and the noise associated with the optical fringes. Sinusoidal modulation was tried in this case, but a significant WMS peak was not observable in the signal. The simulation also showed that the WMS signal for the CO and $CO_2$ mixture is one order of magnitude smaller than the signal for CO.

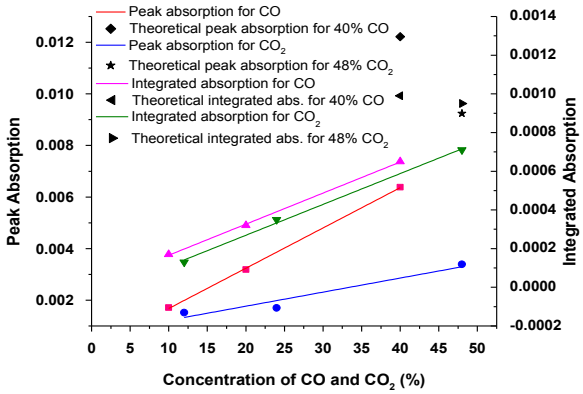


**Figure 11: (a) A comparison of peak and integrated absorption for different concentrations of CO and $CO_2$**

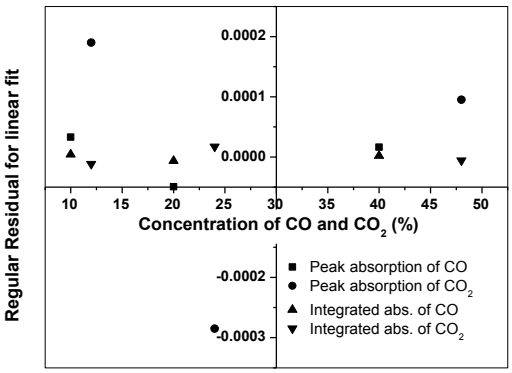


**Figure 11: (b) The deviations of peak and integrated absorption from linear fit for different concentrations of CO and $CO_2$**

*3.2.6. Experiments with three different combinations of concentrations of CO & $CO_2$.* The same cell as used in section 3.2.5 was filled with three different mixtures at 1.2 bar and at 296 K: 10% CO, 12% $CO_2$ , 78% $N_2$; 20% CO, 24% $CO_2$ , 56% $N_2$; and 40% CO, 48% $CO_2$ , 12% $N_2$. The peak absorption and integrated absorption results for CO and $CO_2$ are plotted in figure 11(a), showing that the $CO_2$ absorption spectrum is wider than that of CO as is evident from figure 10. The peak absorption value from the experimental absorption curve is 0.006 lower than that from the theoretical absorption curve both for CO and $CO_2$.

The graph in figure 11(a) shows that the absorptions, both peak and integrated, vary linearly with concentration of CO and $CO_2$. Figure 11(b) shows the deviation of the absorption values from the linear fit. One of the important criteria to gauge the quality of the Auto-DGB process is the difference between the theoretical peak absorption value and the measured one. The Auto-DGB integrated absorption results are closer to the theoretical values for absorption lines of higher linewidth. This is encouraging for measurements of higher linewidth near atmospheric pressure, as in the case for combustion exhaust.

## 4. Discussion

Table 1 shows a comparison among different methods and their detection limits (with associated bandwidths) achieved by different groups. The NES calculated for CO using the simplest implementation of Auto-DGB, i.e. without sinusoidal modulation (subsection 3.2.3), is obtained from the standard deviation value of CO absorption, 0.00011. For 2-f WMS, the equivalent absorptions for the minimum detection limits of concentrations equivalent to noise are cited. The averaging time for the WMS technique is very high, preventing its use for high-bandwidth measurement.

| Methods | References | Species | NES (absorbance $Hz^{-1/2}$) | Averaging time (s) |
|---|---|---|---|---|
| Direct absorption | Wang et al (2000) | CO | $1 \times 10^{-4}$ | 0.1 |
| BRD | Allen et al (1995) | $N_2O$ | $1.6 \times 10^{-6}$ | 10 |
| | Wehe et al (2003) | CO | $5 \times 10^{-6}$ | 0.01 |
| | So et al (2006) | CO | $1 \times 10^{-3}$ | 1 |
| 2-f WMS | Weber et al (2002) | NO | $1.2 \times 10^{-4}$ | 50 |
| | Andersson et al (2007) | $O_2$ | $4.5 \times 10^{-5}$ | 20 |
| | Wang et al (2000) | CO | $1.3 \times 10^{-6}$ | 0.4 |
| Auto-DGB | | CO | $3.6 \times 10^{-6}$ | 0.001 |

**Table 1: A comparison of the NES and averaging time obtained by different groups, using different measurement techniques**

The NES achieved by the BRD technique is equivalent to that of our measurement. (In the case of Allen et al. (1995), the value quoted here takes proper account of their stated bandwidth.) However, the instruments used for BRD operate with typical bandwidth of order 1 Hz. Though NES is calculated taking the bandwidth into account, it does not mean that instruments of the same NES can operate at the same bandwidth.

The measurement artefacts observed in the wings of the measured spectra using Auto-DGB (e.g. Figures 7, 8) merit further work, given their apparent magnitude. Their source remains to be determined, but one possibility is that they arise from interaction between the time constants of the PI feedback control and the transfer function of the measurement system. They are thought to be more prominent in the $CO_2$ absorption spectrum (e.g. Figure 7) compared to CO (e.g. Figure 8) because of the narrow line-width of the former, which results in a fast decrease in the absorption as the laser is scanned through the feature.

It is clearly seen that the Auto-DGB technique can produce the target precision for CO at 1 kHz measurement bandwidth.

**5. Conclusions**

The new technique of Auto-Digital Gain Balancing has been presented. Auto-DGB is a radical extension of the concept of balanced detection (for noise reduction). It uses a digital balancing technique where the balance is expressed in the gain applied by a feed-back loop. The gain is applied to the *error* signal of the balance, and since it is applied by a multiplying DAC whose gain range can be refined in every iteration, the degree of balance is limited by electronic noise effects, rather than optical noise effects. The above approach represents a step-change in measurement science.

Auto-DGB has been applied for several measurements of absorption lines of CO and $CO_2$. Even without any further noise reduction mechanisms, Auto-DGB shows the capability to achieve the target sensitivity (precision 0.0001) in CO absorption over a 50mm pathlength, at kHz bandwidths. In some demonstrations, the laser scan range included a $CO_2$ absorption line, and Auto-DGB provided measurements of *both* species in a single scan. From the experimental results in section 3, it is clear that further analysis of complete lineshapes would improve the Auto-DGB results further.

It is important to explore further the use of techniques such as lock-in measurement, and the robust engineering design of a multi-channel system. The electronic scheme for Auto-DGB is, in principle, readily replicated for many measurement channels. The same measurement scheme is to be extended to the mid-IR range using QCL for achieving 10 ppm measurement. The remaining requirement, therefore, to enable implementation of a tomographic beam array to meet the specification, is to define a viable mid-IR optics system.

Auto-DGB will have many other applications, including the measurement of very weak absorbers at high concentrations. One such case is $O_2$, simultaneous imaging of which with hydrocarbon fuel would enable direct imaging of air-fuel ratio in combustion systems.

## Acknowledgements

SP is grateful for the financial support from the School of Electrical & Electronic Engineering, the EPSRC via Platform Grant EP/D031117/1, the Virtual Centre for Industrial Process Tomography, and the Worshipful Company of Scientific Instrument Makers. HMcC gratefully acknowledges interesting discussions with Johnson Matthey plc, and the support of this work by EPSRC through grant EP/D031117/1. SP is very grateful to Dr. Paul Wright, University of Manchester, for fruitful discussion at the time of execution of the project.

## 6. References

Allen M G, Carleton K L, Davis S J, Kessler W J, Otis C E, Palombo D A, and Sonnenfroh D M 1995 Ultrasensitive dual-beam absorption and gain spectroscopy: applications for near-infrared and visible diode laser sensors *Appl. Optics* **34** 3240-3249

Andersson M, Persson L, Svensson T, and Svanberg S. 2007 Flexible lock-in detection system based on synchronised computer plug-in boards applied in sensitive gas spectroscopy *Rev. Sc. Inst.* **78** 113107

Barrass S, Gérard Y, Holdsworth R J, and Martin P A 2004 Near-infrared tunable diode laser spectrometer for the remote sensing of vehicle emissions *Spectrochimica Acta Part A* **60** 3353–3360

Hafiz R and Ozanyan K B 2007 Digitally balanced detection for optical tomography *Rev. Sc. Inst.* **78** 103101

Hindle F P, Carey S J, Ozanyan K B, Winterbone D E, Clough E and Mccann H 2001 Measurement of Gaseous Hydrocarbon Distribution by a Near-Infra-Red Absorption Tomography System *Journal of Electronic Imaging* **10** 593-600

Hobbs P C D 1990 Shot-noise limited optical measurements at baseband with noisy laser in ROY R. (ed.) *Laser Noise Proc. SPIE* **1376** 216–221

Hobbs P C D 1997 Ultrasensitive laser measurements without tears *Appl. Opt.* **36** 903-920

Kayes D and Hochgreb S 1996 Development of a Time and Space Resolved Sampling Probe Diagnostic for Engine Exhaust Hydrocarbons *SAE No.* 961002

Kluczynski P and Axner O 1999 Theoretical description based on Fourier analysis of wavelength-modulation spectrometry in terms of analytical and background signals *Appl. Opt.* **38** 5803-5815

Kluczynski P, Gustafsson J, Lindberg A, and Axner O 2001a Wavelength modulation absorption spectrometry - an extensive scrutiny of the generation of signals *Spectrochim. Acta. Part B* **56** 1277–1354

Kluczynski P, Lindberg A, and Axner O, 2001b Background signals in wavelength-modulation spectrometry with frequency-doubled diode-laser light. I. Theory *Appl. Opt.* **40** 783–793

Kluczynski P, Lindberg A, and Axner O 2001c Background signals in wavelength-modulation spectrometry by use of frequency-doubled diode-laser light. II. Experiment *Appl. Opt*. **40** 794–805

Koltsakis GC and Stamatelos AM 1997 Catalytic Automotive Exhaust Aftertreatment *Prog. Energy Combust. Sci.* **23** 1-39

Li H, Rieker G B, Liu X, Jeffries J B, and Hanson R K 2006 Extension of wavelength-modulation spectroscopy to large modulation depth for diode laser absorption measurements in high-pressure gases *Appl. Opt.* **45** 1052-1061

Liu J T C, Jeffries J B, and Hanson R K 2004 Wavelength modulation absorption spectroscopy with 2f detection using multiplexed diode lasers for rapid temperature measurements in gaseous flows *Appl. Phys. B* **78** 503–511

Noxon J 2006 *Topology and Noise Using Multiplying DAC* Texas Instruments Application Report SBAA146

Pal S, Ozanyan K B and Mccann H 2008a An approach to tomographic measurement of carbon monoxide at minor concentrations *Meas. Sci. Technol.* **19** 094018

Pal S, Wright P and Mccann H 2008b Digital gain balancing technique for sensitive detection of minor gas concentrations *Proc. 15th IEEE ICECS* (Malta, 31st August – 3rd September, 2008) 858 – 861

Pal S 2009 Sensitive Detection Techniques and Systems for Minor Species Tomography *PhD Thesis* University of Manchester

Rothman L S et al 1996 The HITRAN molecular spectroscopic database and hawks (hitran atmospheric workstation): 1996 edition *J. Quant. Spectrosc. Radiat. Transfer* **65**(5) 665-710

Rothman L S et al 2005 The HITRAN 2004 molecular spectroscopic database *J. Quant. Spectrosc. Radiat. Transfer* **96** 139-204

Schweich D, Flow, heat and mass transfer in a monolithic catalytic converter, *Catalysis and Automotive Pollution Control II : Proc. Of 2nd Intl. Symp. CAPoC2, (*Brussels, September 10-13, 1990) 437-464.

So S G, Wysocki G, Frantz J P, and Tittel F K 2006 Development of Digital Signal Processor controlled Quantum Cascade Laser based Trace Gas Sensor Technology *IEEE Sensors Journal* **6** 1057-1067

Sonnenfroh D M and Allen M G 1996 Ultrasensitive, visible tunable diode laser detection of $NO_2$ *Appl. Opt.* **35** 4053-4058

Sonnenfroh D M, Rawlins W T, Allen M G, Gmachl C, Capasso F, Hutchinson A L, Sivco D L, Baillargeon J N and Cho A Y 2001 Application of balanced detection to absorption measurements of trace gases with room-temperature quasi-cw qc lasers *Appl. Opt.* **40** 812-820

Stone R 1999 *Introduction to Internal Combustion Engines* (London: Macmillan Press) 3rd edition
Sutela C, Collings N and Hands T 1999 Fast Response CO2 sensor for Automotive Exhaust Gas Analysis *SAE No.* 1999-01-3477
Terzija N, Davidson J L, Garcia-Stewart C A, Wright P, Ozanyan K B, Pegrum S, Litt T J and McCann H 2008 Image optimisation for chemical species tomography with an irregular and sparse beam array *Meas. Sci. Technol.* **19** 094007
Wright P, Ozanyan K B, Garcia-Stewart C A, Carey S J, Hindle F P, Hurr W, Pegrum S, Colbourne S, Turner P, Crossley S D, Litt T, Murray S C, and McCann H 2005a Toward In-Cylinder Absorption Tomography in a Production Engine *Appl. Opt.* **44** 6578-6592
Wright P, Ozanyan K B, Carey S J, and McCann H, 2005b Design of High-Performance Photodiode Receivers for Optical Tomography *IEEE Sensors J.* **5** 281-288
Wright P, Terzija N, Davidson J L, Garcia-Castillo S, Garcia-Stewart C A, Pegrum S, Colbourne S, Turner P, Crossley S D, Litt T J, Murray S C, Ozanyan K B and McCann H 2010 High-speed Chemical Species Tomography in a multi-cylinder automotive engine *Chem. Eng. J.* **158** 2-10
Wang J, Maiorov M, Baer D S, Garbuzov D Z, Connolly J C, and Hanson R K 2000 In situ combustion measurements of CO with diode-laser absorption near 2.3 μm *Appl. Opt.* **39** 5579-5589
Weber W H, Remillard J T, Chase R E, Richert J F, Capasso F, Gmachl C, Hutchinson A L, Sivco D L, Baillargeon J N, and Cho A Y 2002 Using a wavelength-modulated quantum cascade laser to measure NO concentrations in the parts-per-billion range for vehicle emissions certification *Appl. Spec.* **56**(6) 706-714
Wehe S, Allen M, Liu X, Jeffries J, and Hanson R 2003 Room-temperature mid-IR lasers for on-line measurements of trace combustion generated pollutants *Proc. IEEE Sensors* p795-800
Zhu X and Cassidy D T 1995 Electronic subtractor for trace-gas detection with InGaAsP diode lasers *App. Opt.* **34** 8303-8308